Gold Nanorods Indirectly Promote Migration of Metastatic Human Breast Cancer Cells in Three-Dimensional Cultures

Elissa M. Grzincic and Catherine J. Murphy*

Department of Chemistry, University of Illinois at Urbana—Champaign, Urbana, Illinois 61801, United States

ABSTRACT Gold nanomaterials are intensively studied for applications in disease detection, diagnosis and therapeutics, and this has motivated considerable research to determine their interaction with biomolecules, cells and cell behaviors. However, few studies look at how nanomaterials alter the extracellular matrix (ECM) and cell—ECM interactions. Nanomaterials in the body would interact with the entire cellular environment, and it is imperative to account for this when studying the impact of nanomaterials on living systems. Furthermore, recent evidence finds that migration rates of cells in 2D can be affected by nanomaterials, and uptake of the nanomaterials is not necessary to exert an effect. In this study, three-dimensional nested type I collagen matrices were utilized as a model ECM to study how gold nanorods affect the migration of MDA-MB-231 human breast cancer cells. Spontaneous cell migration through collagen containing gold nanorods was found to increase with increasing concentrations of gold nanorods, independent of intracellular uptake of the nanorods. Gold nanorods in the collagen matrix were found to alter collagen mechanical properties and structure, molecular diffusion, cellular adhesion, cell morphology, mode of migration and protease expression. Correlation between decreased cellular adhesion and rounded cell morphology and locomotion in nanorod-containing collagen suggests the induction of an amoeboid-like migratory phenotype.

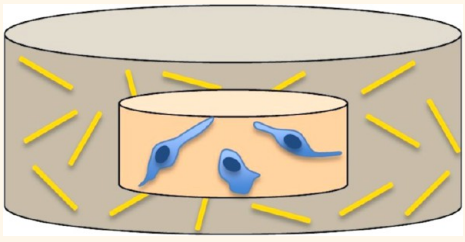

KEYWORDS: gold nanorods · extracellular matrix · collagen · migration · MDA-MB-231 · breast cancer

In the past few decades, nanomaterials have become highly prevalent in the biomedical research community for a wide range of applications.[1] Gold nanorods (AuNRs) in particular are uniquely suited for numerous biological applications due to both their optical and physical properties.[1−3] These relatively chemically inert, plasmonic nanoparticles (NPs) are being investigated for use in biomedical imaging, tracking and sensing, drug and gene delivery, and photothermal therapy of cancer.[1−10] Moreover, the optical properties of AuNRs can be tuned throughout the near-IR "water window" region by facile and scalable synthetic strategies, and interactions with biomolecules can be modulated *via* surface functionalization.[10−12]

Because of the pervasiveness of nanomaterials in medicine, much research has focused on the fundamental understanding of how NPs interact with cells on the molecular and organismal levels. There exists substantial data on the cellular uptake and accumulation of gold NPs and their effect on simple cell behaviors such as survival and proliferation.[13−16] It is being increasingly recognized that the "protein corona" plays a large role in the impact of NPs on cells.[17−19] Recently, our group and others have studied the effect of gold NPs on cell migration, an essential process in embryogenesis, wound healing and cancer cell metastasis.[20] We found that gold NPs of various shapes and surface coatings deposited on a surface inhibited two-dimensional (2D) cell migration of PC3 cells, while shape and surface coating determined the effect on HDF cell migration.[21] Positively charged gold nanospheres and AuNRs increased migration rates of HDF cells, while PEGylated gold nanospheres and AuNRs inhibited migration.[21] Negatively charged gold nanospheres inhibited migration while negatively charged AuNRs enhanced migration in these cells.[21] Others have shown AuNRs to inhibit 2D migration of MDA-MB-231, PC3 and B16F10 cells after

* Address correspondence to murphycj@illinois.edu.

Received for review October 27, 2014 and accepted June 29, 2015.

Published online June 29, 2015
10.1021/acsnano.5b03362

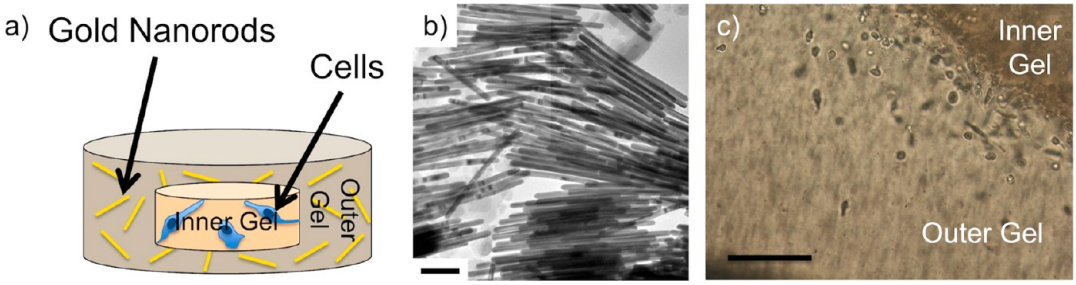

Figure 1. (a) Schematic of 3D nested collagen gels for migration assays. The inner gel contains 200 000 cells/mL and the outer gel contains up to 3 × 10^{10} rods/mL. (b) Transmission electron micrograph of aspect ratio 18 AuNRs used in outer gels (scale bar = 100 nm). (c) Example brightfield micrograph of cells migrating from inner gel to outer gel in 3 × 10^{10} rods/mL sample (scale bar = 200 μm).

NP cellular uptake.[22] Other types of NPs were shown to inhibit cell migration as well.[23] All of these studies have suggested that nanoparticles alter cellular adhesion to the substrate. Furthermore, NPs in collagen matrices have been shown to alter cellular phenotypes in cardiac fibroblasts, possibly due to the ability of NPs to adsorb soluble factors from the environment.[24,25]

Cell migration is a highly matrix-dependent process and 2D studies have not taken the extracellular matrix (ECM) into account when observing migrating cells exposed to gold NPs.[26−28] Typical cell migration through fibrillar matrices (fibrillary type I collagen is the main structural component present in ECM of connective tissue) occurs as a cycle.[29] Leading edge protrusions form and focal adhesion in the front and rear of the cell cause cell elongation.[29] This is accompanied by proteolytic ECM breakdown, followed by rear-end contraction and matrix detachment to move the cell forward.[29] Not only is the typical process of proteolytic matrix degradation not observed in 2D migration studies on hard tissue culture plastic, but the role of substrate adhesions in movement is altered. The importance of adhesion contacts in cell migration is actually 2-fold: they allow cells both to generate traction forces and to sense their mechanical environment.[30,31] ECM mechanical properties and microstructure have been shown to be critical factors in the metastatic potential of tumor cells (particularly in breast cancer)[32] as these factors determine the level of steric hindrance cells experience, whether the cells can deform the matrix, and the diffusion of soluble biochemical factors.[26−34] Furthermore, mechanotransduction pathways allow cells to "feel" changes in these properties from a distance and respond directly in a myriad of ways.[34−37] AuNRs injected into the body for any application would not only come into contact with a large assortment of cell types, but also with the three-dimensional (3D) ECM containing structural and soluble proteins. NPs themselves are known to adsorb soluble biochemical factors in cellular environments; therefore, they have the potential to alter signaling gradients in 3D matrices that trigger cells to migrate.[17−19,25,38] Accordingly, the interplay of AuNR-ECM interactions is a largely missing dimension in the study of cell-AuNR interactions.

In order to study the effect of AuNRs in the ECM on cell migration, we have mimicked the ECM of MDA-MB-231 human breast cancer cells with 3D type I collagen cell cultures, then measured spontaneous cell migration through an outer layer of collagen with and without AuNRs. Type I collagen is a ubiquitous component of the ECM and self-assembled type I collagen produces a soft mammary gland-like environment ideal for MDA-MB-231 cells.[39] In addition to comparing average frequency of migration in these cell populations, we also measured other factors involved in cell migration, including the morphology of the migrating cells, locomotion mechanism, β1-integrin expression, overall cell adhesion and matrix metalloproteinase expression. The microstructure and mechanical properties of the 3D collagen gels with and without AuNRs were studied in order to measure changes that might alter the ability of cells to move through or deform the matrix. Additionally, we measured molecular diffusion rates through gels containing different AuNR concentrations to determine whether the 3D porous collagen/AuNR structure could alter biochemical gradients of soluble factors.

RESULTS

Spontaneous Migration of MDA-MB-231 Cells is Enhanced through 3D Collagen Matrices Embedded with Gold Nanorods. MDA-MB-231 cells were chosen due to their high mobility and metastatic potential. Type I collagen was used not only because is it a good choice for mimicking a simple fibrous matrix for this cell type, but also because its transparency makes it ideal for live cell imaging. In order to culture MDA-MB-231 cells in a biomimetic 3D environment while still being able to measure migration of whole populations, we used a 3D nested gel matrix design (Figure 1a).[40,41] This allowed us to surround a 3D cell culture ("inner gel") with a secondary collagen gel containing AuNRs (no cells) at various concentrations ("outer gel"). This structure created a clear interface between the inner and

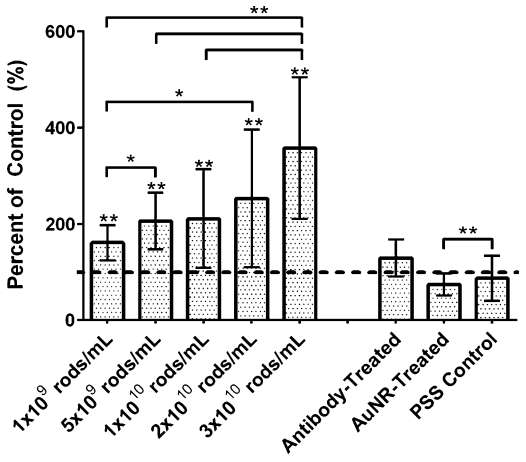

Figure 2. 3D migration assay results showing the average number of migrating cells counted per gel sample (n = 12) as percent of control (control = without AuNRs or any other treatment) for each of the AuNR concentrations tested and antibody-treated, AuNR-treated and PSS controls. Error bars represent standard deviation. The standard deviation of the control for 1 × 10^9 rods/mL through 3 × 10^{10} rods/mL samples is 48.6%, for antibody-treated and AuNR-treated samples is 48.7% and for PSS control samples is 3.7%. The dashed line indicates 100% (average of control) for reference. *p < 0.05, **p < 0.01 (brackets indicate the p-value between two sample types, no bracket = relative to control).

outer gels that was used as a boundary condition for counting how many cells had migrated from the inner gel to the outer gel (Figure 1c). The AuNRs used in these experiments are aspect ratio 18 (~280 nm by ~16 nm) AuNRs triple-coated in polyelectrolytes so that the final layer is a negatively charged layer (polystryene sulfonate, PSS) (Figure 1b). These AuNRs were chosen for this study because they are known to induce changes in type I collagen mechanical properties and to alter the ability of cardiac fibroblasts to contract 3D collagen gels.[24,42] The AuNRs were added to the liquid neutralized collagen solution immediately before curing into a gel at 37 °C. Collagen/AuNR environments were nontoxic at all concentrations to the cells (Figure S1, Supporting Information). The incubation of preformed collagen gels in AuNR solutions led to little incorporation of the nanorods into the gels. However, as cells are continually remodeling their ECM, it is not unreasonable to expect that nanoparticles in the ECM could be exposed to cells.[39,43]

The migration experiments were run over a range of five different AuNR concentrations from 1 × 10^9 rods/mL of collagen solution (~1.7 pM) to 3 × 10^{10} rods/mL (~50.0 pM) and control samples containing no AuNRs. The experiments lasted 4 days to allow sufficient spontaneous cell migration from the inner to the outer gels and 12 separate gels were analyzed for each AuNR concentration over four separate experiments. The results are shown in Figure 2: as the concentration of AuNRs in the outer gel increases, the number of cells that spontaneously migrate from the inner gel to the outer gel increases. This biological action-at-a-distance effect of NPs on cells is unprecedented. We hypothesize that the mechanism(s) by which AuNRs in collagen enhance spontaneous migration is by (a) changing the mechanical and structural properties of the collagen gel networks and/or (b) altering biochemical gradients, both in a migration-favored manner.

The cellular uptake of AuNRs alone has been inferred to alter the migration of cells in 2D experiments.[21−23] In 3D, it was not clear to what extent this observation would hold. The inner gel/outer gel geometry was chosen to make measurement of cell migration and direction relatively easy; in addition, this geometry allows distinct chemical and mechanical environments for cells to sample in 3D. Cells were found to uptake some AuNRs after 4 days when well-mixed with AuNRs in 3D collagen gels, indicating that cells migrating from the inner to the outer gel can pick up AuNRs as they move (*via* confocal imaging, Figure S2). ICP-MS experiments to rigorously quantify the degree of AuNR uptake failed, due to problems in separation of gel-bound rods from cell-bound rods (see Materials and Methods). As an alternate approach, migration studies with cells that had previously uptaken large numbers of AuNRs (~32 000 AuNRs per cell by ICP-MS) before being cast into the collagen gels were performed. The outer gel for these samples was then pure collagen, with no additional AuNRs. The migration of "AuNR-treated" cells was found to have negligible difference from controls, as seen in Figure 2. Therefore, it appears that in 3D, merely bearing a load of nanoparticles does not impact cell migration (in terms of numbers of cells that move across a boundary, not rate).

Another mechanism by which AuNRs could alter cell migration is if they blocked the cellular machinery that makes physical contact to collagen; the principal cell surface protein that binds to type I collagen is β1-integrin.[44] To test the role of β1-integrin adhesion in the observed migration changes, migration of cells that had been pretreated with anti-β1-integrin blocking antibody was also measured in the inner gel/outer gel setup ("antibody-treated"). These samples showed a slight increase in migration compared to controls, but these results are statistically insignificant. This data might suggest that "integrin fouling" is not the primary determinant in the change in cellular behavior, but this assumes that the number of integrins per cell is constant. This is not the case; there appear to be fewer integrins per cell once the cells have "seen" nanorods (see below). Lastly, to determine if observed migration changes could be due simply to the PSS coating of the AuNRs and not the AuNRs themselves, controls in which the outer gel contained excess PSS (0.1 mg/mL, based on a rough estimate of PSS content on the AuNRs, see Materials and Methods section) were analyzed and negligible difference from control was measured in this

case as well. These three types of samples/controls were first tested by live/dead analysis for consistency (Figure S3). For all subsequent experiments, both AuNR-treated and antibody-treated samples were analyzed for both consistency in controls and additional information about the possible mechanisms of action.

Cells Become Rounded in the Presence of Collagen Gels Containing Gold Nanorods. In order to understand how overall cell migration is increased in collagen/AuNR gels, characterization of the entire system (cells and matrix) was done (Figure 3). We first characterized the migrating cells in ways that are relevant to different parts of the cell migration cycle (mode of migration, adhesion, proteolysis). First, we compared the morphology of cells that had migrated into an outer gel containing no AuNRs (control) and cells that had migrated into a 3×10^{10} rods/mL outer gel by brightfield microscopy and confocal fluorescence microscopy (Figure 4). It was observed that more of the migrated cells in the AuNR-containing gels were in a rounded morphology and tended to be more detached from neighboring cells than in controls.

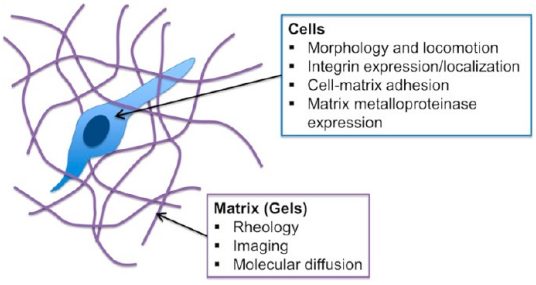

Figure 3. Characterization techniques used for understanding influence of gold nanorods on cell-matrix interactions and cell migration.

To quantify the difference in morphology, we measured the aspect ratio of 600 cells from random brightfield micrographs to obtain a measure of "roundness" (Figure 4e).[45] It was found that the cells in the AuNR-containing gel were significantly more rounded on average (mean aspect ratio/"elongation factor" was 4.3 for collagen samples and 2.1 for collagen/AuNR samples). Additionally, AuNR-treated cells and antibody-treated cells migrating into collagen outer gels had a mean elongation factor of 4.4 and 3.7, respectively (Figure S4). The difference in elongation factor from controls for AuNR-treated cells was insignificant, but the antibody-treated cells showed slight rounding relative to controls ($p = 0.012$) to land in between the measurement for cells in collagen and collagen/AuNR samples.

Using time-lapse brightfield microscopy, we were able to observe that cells in the AuNR-containing gel constructs actually migrated in a rounded fashion. Rather than the cyclic elongation-contraction normally migrating control cells exhibit, cells migrating through AuNR-containing collagen seem to propel themselves forward without elongation. Videos constructed from time-lapse microscopy experiments are available as Supporting Information (Movie S1−S3) with Movies S2 and S3 containing green overlaid circles to indicate some cells exhibiting rounded locomotion; chronological images of a representative control cell and rounded cell moving are shown in Figure 5 (a and b respectively). Movies S4 and S5 are also included of antibody-treated and AuNR-treated cells migrating into collagen outer gels. Mesenchymal or fibroblast-like migration is the term for the typical cyclic migration of cells.[45−48] These cells first produce leading edge protrusions, which are stabilized by binding to the ECM

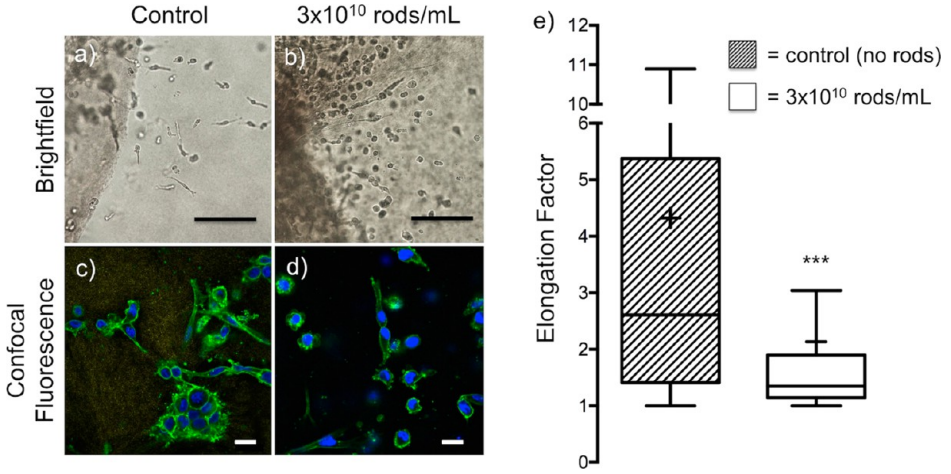

Figure 4. (a) Representative micrograph of cells that had migrated from the inner gel to the outer gel without AuNRs (control) and (b) with 3×10^{10} rods/mL after 4 days (scale bars = 200 μm). (c) Representative confocal fluorescence micrograph of cells that had migrated from the inner gel to the outer gel without AuNRs (control) and (d) with 3×10^{10} rods/mL after 4 days. Cells are stained for F-actin (green) and nuclei (blue). Scale bars = 20 μm. (e) Box-and-whisker plots of elongation factor (aspect ratio) distribution of migrated cells in collagen (striped) and 3×10^{10} rods/mL collagen (white) samples. Center line denotes median, top and bottom boxes are 75th and 25th percentiles, whiskers are inner fence limits (1.5 interquartile range, with cutoff at 1.0 since as a minimum) and plus sign marks the mean elongation factor. $n = 300$, $^{***}p < 1.0 \times 10^{-10}$.

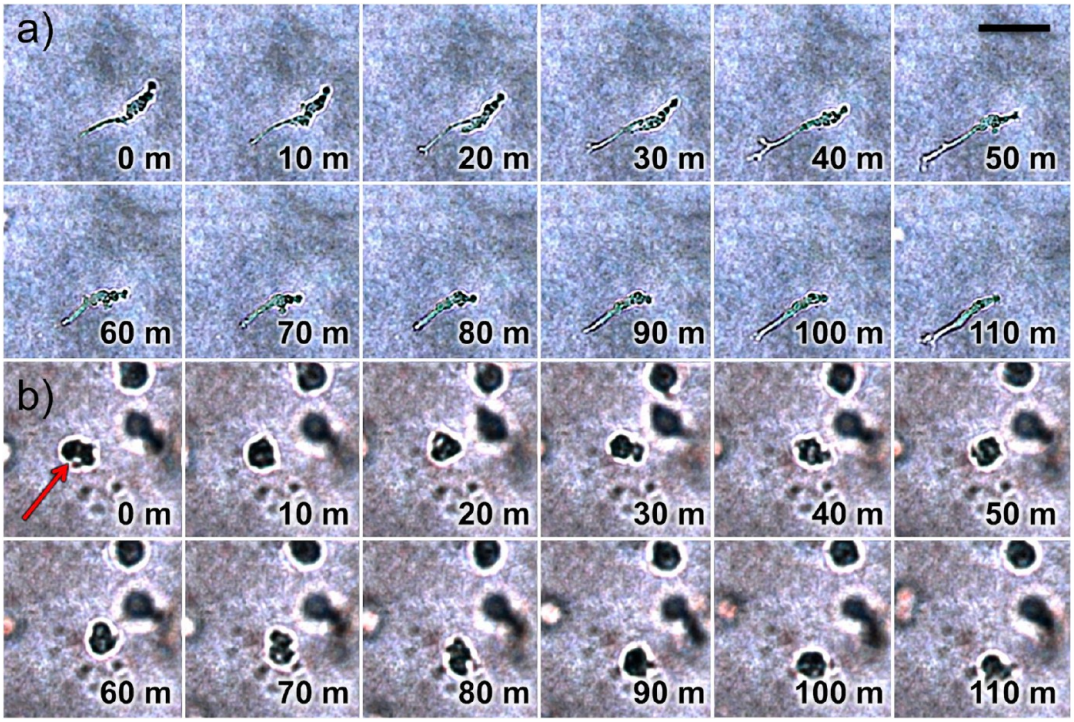

Figure 5. Chronological series of brightfield micrographs from time-lapse experiments showing (a) normally migrating cell moving through collagen (from Movie S1) and (b) round migrating cell moving through 3×10^{10} rods/mL collagen (from Movie S2). Scale bar = 50 μm. Bottom right corner of each image denotes time duration in minutes. Red arrow shows cell of interest.

via integrin receptors, inducing integrin clustering and focal adhesion formation.[27,45−48] These adhesion sites serve as traction sites as the cells moves forward over them, and then they are disassembled at the cell rear, allowing it to detach and contract.[27,45−48] However, sometimes tumor cells can go through a reversible mesenchymal-amoeboid transition where they can quickly switch to an amoeboid mode of migration depending on environmental conditions.[45−48] The most obvious characteristic difference between the mesenchymal and amoeboid moves are that amoeboid cells are rounded.[45−48] Rather than extending protrusions with the force of actin polymerization, amoeboid cells use the flexibility of their cytoskeletons to propel and squeeze themselves through the ECM with low or nonexistent adhesion to the matrix.[45−48] In addition to the rounded nature of migration, amoeboid cells are characterized by lack of integrin clustering, lack of protease activity (as the cells squeeze through existing space in the ECM and do not need to break it down), changes to RhoA-ROCK and Rac signaling pathway activation, and locomotion velocity.[45−48] On the basis of morphology and time-lapse videos, the movement observed in the AuNR-containing gels seems to be an example of amoeboid migration. A mesenchymal-amoeboid transition has been documented in the literature to occur many times in cancer cells, including this specific cell type, under protease-blocking conditions.[45,49,50]

The Presence of Gold Nanorods Is Correlated to Decreased Cellular Adhesion to the Matrix. To further investigate the possibility of a mesenchymal-amoeboid transition occurring when cells migrate through AuNR-containing collagen matrices, we then measured the ability of cells to adhere to the collagen. Changes to the ECM stiffness and density also influence the ligand density, thus the ability of cells to adhere to the network.[46−48] Amoeboid cells are characterized by reduced cellular adhesion and diffuse, unclustered integrins.[46−48] Figure 6 shows representative images of migrating cells in control gels (no AuNRs, Figure 6a−c) and in gels containing 3×10^{10} rods/mL (Figure 6d−f). These cells are immunostained for β1-integrins and that signal is shown in green (blue in some images is from DAPI staining). β1-integrins were chosen for analysis because the two main type I collagen integrin receptors both contain β1 components.[44] Images were collected at the same parameters. It was found that in control samples, cells had much higher β1-integrin expression overall and extensive integrin clustering was observed in most cells. In contrast, in cells migrating through AuNR-containing collagen, very low β1-integrin signal was observed and the integrins are very diffuse throughout the entire membrane (no clusters observed). This is consistent with decreased focal adhesion formation and amoeboid migration. AuNR-treated cells appear very similar to control images (Figure S5).

To directly measure cellular adhesion, collagen and collagen/AuNR gels were formed and cells were

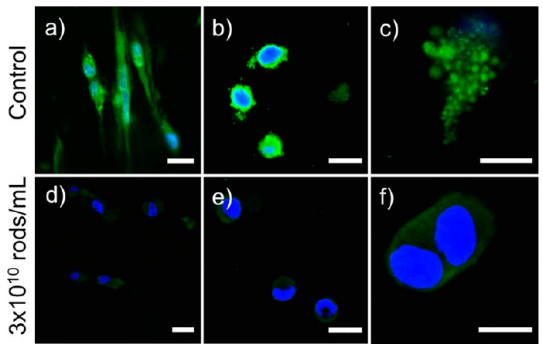

Figure 6. Confocal fluorescence micrographs of migrating cells in (a−c) collagen and (d−f) 3 × 10^{10} rods/mL collagen gels, stained with FITC-tagged P5D2 anti-β1-integrin antibody (green) and DAPI (blue). Representative images were collected at same imaging parameters between samples for ~300 cells. Scale bars are (a) 20 μm, (b) 20 μm, (c) 10 μm, (d) 20 μm, (e) 20 μm, and (f) 10 μm.

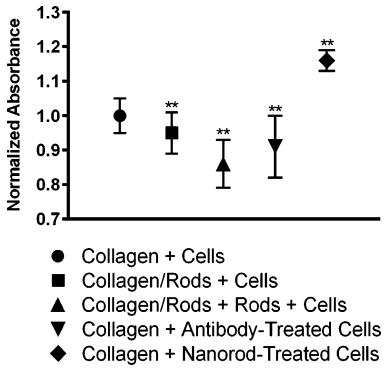

Figure 7. Averaged normalized absorbance of *p*-nitro-pheno-*N*-β-D-glucosaminide, which is proportional to number of adhered cells, for each type of sample tested. Circle = cells adhered to collagen, square = cells adhered to 3 × 10^{10} rods/mL collagen, triangle = cells adhered to 3 × 10^{10} rods/mL collagen with additional AuNRs deposited on top of gel before addition of cells, upside-down triangle = P5D2 β1-integrin blocking antibody-treated cells adhered to collagen and diamond = cells that had previously been exposed to 3 × 10^{10} rods/mL medium before adhering to collagen. n = 8, **p < 0.001 relative to control.

allowed to adhere to the tops. By washing away free, unattached cells and then staining the still-adhered ones, we acquired a relative measure of cellular adhesion proportional to absorbance of the dye (Figure 7).[51] The dye used was *p*-nitro-pheno-*N*-β-D-glucosaminide, which only turns yellow when metabolized by *N*-acetyl-β-D-glucosaminidase in live cells (absorbance is linearly related to cell number over a wide range).[51] We tested cellular adhesion to control collagen gels (circle in Figure 7) and to collagen/AuNR gels (3 × 10^{10} rods/mL, square in Figure 7). Additionally, to determine if any differences in adhesion between collagen and collagen/AuNR gels were solely due to stiffness/microstructure changes and not the AuNRs themselves, we also tested collagen/AuNR gel samples onto which additional AuNR were allowed to settle on top of the already-formed gels before adding the cells (triangle in Figure 7). As a positive control, cells pretreated with anti-β1-integrin blocking antibody (antibody-treated) were tested on collagen gels (upside-down triangle in Figure 7). To determine if adhesion was altered simply by the uptake of the AuNRs, AuNR-treated cells were also tested on collagen gels (diamond in Figure 7). It was found that cell adhesion was decreased on collagen/AuNR gels and further decreased on collagen/AuNR with additional rods deposited on top. These results confirm that decreased β1-integrin expression and clustering in cells migrating through collagen/AuNR gels is correlated with decreased cellular adhesion. Furthermore, the AuNRs themselves between the cells and the matrix further decrease the ability of cells to adhere and similarly decreased adhesion was measured in antibody-treated cell samples. Cells that had previously uptaken AuNRs actually showed stronger adhesion to collagen gels.

It should be noted that cells used for β1-integrin expression analysis were cultured well-mixed directly in collagen with 3 × 10^{10} rods/mL for the AuNR-containing samples. This was done in order to closely study a large population of cells that model cells that have already migrated, *i.e.*, have already reached the outer gel. The separation of cells and AuNRs into inner and outer gels is a tool for measuring the role of AuNRs in the extracellular environment on the migration of large numbers of cells using a clear starting point. However, for the integrin expression and matrix metalloproteinase expression measurements, it was necessary to mix cells directly with AuNR-containing collagen in order to measure large quantities of only the cells that had ultimately been exposed the outer gel.

Gold Nanorods Up-Regulate Matrix Metalloproteinase Expression but RhoA/ROCK/Rac Is Unchanged. In order to measure the effect of the collagen/AuNRs on the proteolytic process, RNA expression of multiple matrix metalloproteinases (MMPs) were quantified by qPCR in cells that had been cultured in collagen or 3 × 10^{10} rods/mL collagen/AuNR gels for 4 days before RNA extraction. Amoeboid-like migration is typically nonproteolytic migration because cells can move through existing pathways in the collagen network.[45−50] Antibody-treated cells and AuNR-treated cells were also tested as controls, after being cultured in collagen for 4 days. The collagenases MMP1 and MMP13, gelatinases MMP2 and MMP9 and MMP14 (a membrane-bound MMP, also known as MT1-MMP) were tested. The results from qPCR are tabulated in Table 1 (and also graphed as fold change and raw C_t in Figure S6). All five MMPs tested were up-regulated with respect to controls (cells in only collagen), while none were altered with antibody-treated cell samples or with cells that had previously uptaken AuNRs (MMP13 was actually down-regulated in these samples). The up-regulation of proteases by the cells in collagen/AuNR gels is inconsistent with traditional amoeboid-like migration,

TABLE 1. qPCR Results

	collagen/AuNRs[a]		antibody-treated[b]		AuNR-treated[c]	
gene	FC[d]	*p*-value[e]	FC	*p*-value	FC	*p*-value
MMP1	**3.65**	**6.0×10^{-3}**	0.88	5.4×10^{-2}	1.05	0.55
MMP2	**2.60**	**4.0×10^{-3}**	1.07	0.44	1.40	**5.1×10^{-3}**
MMP9	**3.23**	**1.8×10^{-3}**	0.65	**2.8×10^{-3}**	1.14	0.30
MMP13	**2.09**	**2.4×10^{-2}**	**0.50**	**7.0×10^{-3}**	**0.37**	**5.0×10^{-3}**
MMP14	**2.10**	**1.2×10^{-2}**	0.81	0.12	0.76	7.2×10^{-2}
RHOA	1.24	0.26	0.66	**7.8×10^{-3}**	0.54	**4.2×10^{-3}**
RAC1	1.70	0.28	1.68	0.14	1.27	**2.9×10^{-2}**
ROCK1	0.82	0.45	0.79	**1.9×10^{-2}**	0.72	**2.9×10^{-2}**

[a] Samples of RNA from cells cultured in collagen containing 3×10^{10} rods/mL. [b] Samples of RNA from cells treated with P5D2 β1-integrin blocking antibody prior to culture in collagen. [c] Samples of RNA from cells treated with 3×10^{10} rods/mL AuNRs for 24 h prior to culture in collagen. [d] Fold change (FC) is the difference in expression relative to control. For example, FC of 2 means that the expression is 2-fold higher than in controls, and FC of 0.5 means that expression is 2-fold decreased or half the expression than in controls. Up-regulated FCs (FC > 2) and down-regulated FCs (FC < 0.05) are shown in bold. [e] Data considered significant if *p*-value is <0.05. Significant *p*-values highlighted in bold font.

though the amoeboid-like classification is mostly determined by the shape and mode of locomotion.[45−50] Additionally, RhoA, ROCK1 and Rac1 were tested and found to be unaltered relative to control for any of the conditions. Increased Rho/ROCK signaling is associated with high contractility characteristic of amoeboid cell lines and is inhibitive of Rac-driven processes.[45−50] Rac is a regulator of lamellipodia in mesenchymal cells and its deactivation is connected to rounded morphologies.[45−50] The absence of changes detected in the expression of these proteins is also incongruous with amoeboid migration.

Gold Nanorods Make Collagen Gels Stiffer and More Elastic. To explore ways in which the AuNR-collagen interactions contribute to any altered cell-collagen interactions, thorough characterization of the collagen networks themselves was completed. We first performed rheological studies on the collagen/AuNR gels in order to elucidate how ECM properties are changed by the addition of AuNRs (Figure 8). For each sample, the still-liquid collagen solution with varying concentrations of AuNRs was placed in a parallel plate geometry (sample is between an oscillating top plate and a stationary bottom plate) set to 37 °C. the sample polymerization was monitored by watching the increase in the storage and loss moduli (storage modulus is the stored energy, in-phase, elastic component of the stress/strain relationship in viscoelastic materials, while the loss modulus is the measure of energy dissipation and denotes the out-of-phase, viscous component) with time under a sinusoidal shear strain at 2 rad/s and 1% strain for 30 min. Representative data from one control gel and one gel with 3×10^{10} rods/mL is shown in Figure 8a. It was observed that the lag time before significant collagen polymerization (fibrillogenesis) occurs is much shortened with the addition of AuNRs, and this effect was seen with all concentrations of AuNRs tested.

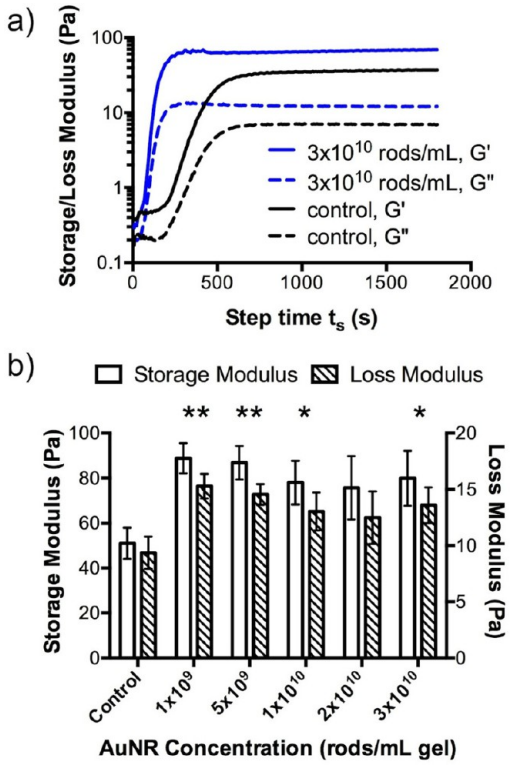

Figure 8. (a) Storage (solid lines) and loss (dashed lines) moduli (Pa) over time (s) for representative control (black lines) and 3×10^{10} rods/mL collagen samples. Still-liquid samples were loaded into rheometer immediately before starting $t = 0$ and allowed to polymerize at 37 °C for 30 min while under oscillations at 2 rad/s and 1% strain. (b) Average storage (white bars) and loss (striped bars) moduli at 1 Hz for each AuNR concentration tested. *$p < 0.05$, **$p < 0.01$ (compared to control samples).

Each sample, after it was allowed to fully polymerized (30 min), was subjected to a frequency sweep from 0.1 to 10 Hz at 1% strain to obtain measurements of final storage and loss moduli across multiple frequencies. The storage and loss moduli for each AuNR concentration at 1 Hz are shown in Figure 8b (full averaged frequency sweep curves are shown in Figure S7). These results show that the collagen becomes stiffer (higher storage modulus) and more elastic (decreased tan(δ), plotted in Figure S8), but that the stiffness and elasticity is not measurably different for different AuNR concentrations.

Gold Nanorods Alter Collagen Gel Structure. Imaging of the microstructure was done by multiple techniques. Confocal reflectance microscopy allowed us to examine the density of collagen fibrils of a wet gel in the same state as during cell culture conditions (Figure 9a, b). When comparing the 3D reconstructed Z-stack images (made by compiling the 80 images taken at 0.4 μm slices), the collagen fibrils (white signal) appear more densely packed, more frequent and shorter in AuNR-containing gels than in control gels. Images from

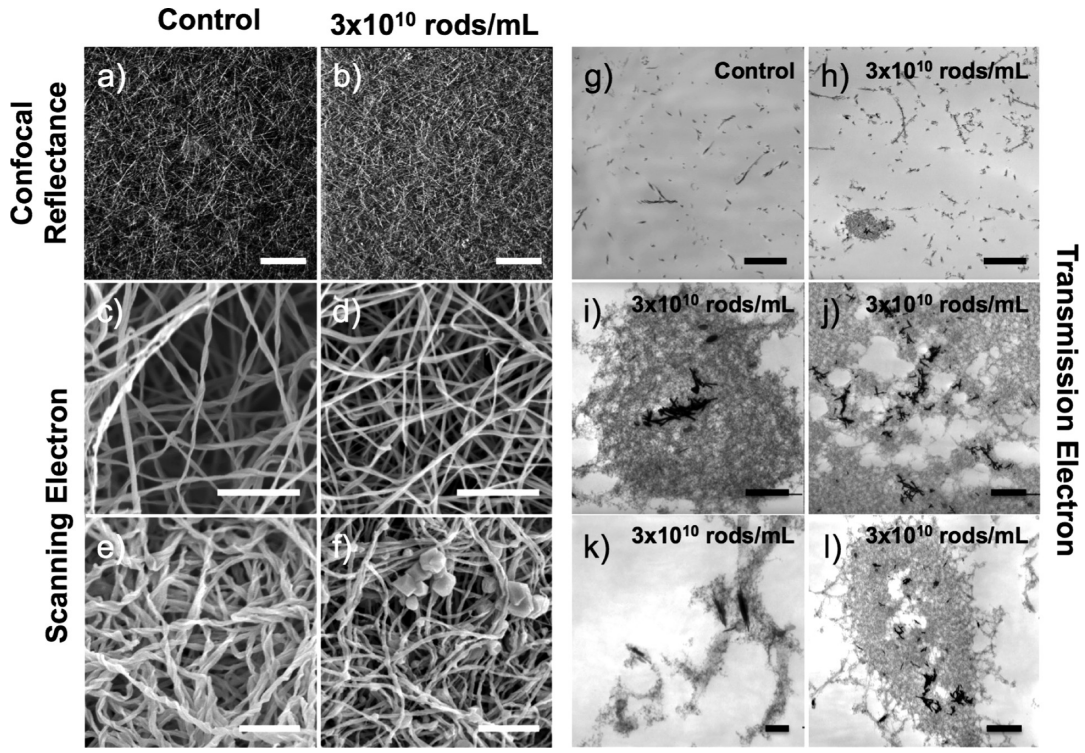

Figure 9. Microscopy of collagen gels with and without AuNRs. Confocal reflectance 3D reconstructed Z-stack image of (a) collagen and (b) 3×10^{10} rods/mL collagen gels (scale bars = 20 μm); scanning electron micrographs of dehydrated (c) collagen and (d) 3×10^{10} rods/mL collagen gels on glass slides (scale bars = 1 μm) and of dehydrated, condensed and sideways-mounted (e) collagen and (f) 3×10^{10} rods/mL collagen gels (scale bars = 1 μm); transmission electron micrographs of (g) collagen samples and (h) 3×10^{10} rods/mL collagen samples (scale bars = 3 μm). (i–l) Increased magnification images of AuNRs in 3×10^{10} rods/mL collagen samples. AuNRs appear black while collagen appears dark gray. Scale bars are (i) 500 nm, (j) 1 μm, (k) 200 nm and (l) 1 μm.

other concentrations of AuNRs can be seen in Figure S9 and the signal increase from the collagen reflectance with increase in AuNR concentration was quantified using ImageJ (Figure S10). Scanning electron microscopy (SEM) was used in order to analyze individual fibrils at much higher magnifications. Figure 9c and 9d are representative SEM images of dehydrated gels on glass slides. By SEM, AuNR-containing gels appear to be denser with shorter, more rigid fibrils. In control samples, often very long, twisted fibrils can be observed and this twisted morphology was never seen in 3×10^{10} rods/mL gels. However, by simply dehydrating collagen samples to use for SEM, we were unable to find any AuNRs. Additional samples were prepared that were dehydrated, condensed and mounted on their sides to image deeper into the polymerized gels. Images of these samples are shown in Figure 9e,f. The same contrasting twisted and rigid fibrils were observed in control and 3×10^{10} rods/mL gels. Additionally, many instances of localized collagen aggregation were found inside the 3×10^{10} rods/mL gels and no AuNRs were located. These collagen aggregations disrupted the collagen networks and it was hypothesized that the AuNRs were actually inside of these aggregations.

To determine the actual location of the AuNRs relative to the collagen fibrils, we performed transmission electron microscopy (TEM) of very thinly sliced collagen gels. In these experiments, control gels contained twisted fibrils and the collagen/AuNR gels contained many more fibrils that were not twisted and large aggregations of collagen (Figure 9g,h). Higher magnification images of the collagen/AuNR gels are shown in Figure 9i–l. These images show how the large aggregations of collagen do seem to contain AuNRs at their center and throughout; no aggregations were found without AuNRs inside. Even where spherical aggregations did not form, where there are large numbers of AuNRs, the collagen network appears to be denser (Figure 9j). There were also many instances of small numbers of AuNRs being associated with singular fibrils as well (Figure 9k).

Gold Nanorods Restrict Diffusion of Positively-Charged Molecules. Finally, to examine how the presence of AuNRs in the collagen might alter molecular diffusion through the gels, we performed fluorescence recovery after photobleaching (FRAP) experiments and visible dye diffusion experiments. The visible dye diffusion experiments (Figure 10) showed that negatively charged dyes are able to pass through both control and collagen/AuNR gels (3×10^{10} rods/mL) at comparable rates, while positively charged dyes are trapped near the top of the collagen/AuNR gels. FRAP experiments with fluorescein, which is negatively charged under conditions used, did not shown much change in the

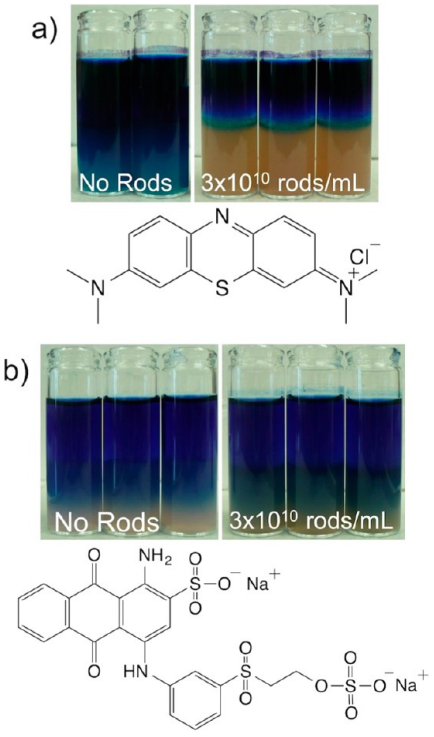

Figure 10. (a) Photographs of collagen samples with 3 × 10^{10} rods/mL (right) or without AuNRs (left) after 8 h of diffusion of 1 mM Methylene Blue (structure shown below). (b) Photographs of collagen samples with 3 × 10^{10} rods/mL (right) or without AuNRs (left) after 8 h of diffusion of 1 mM Remazol Brilliant Blue R (structure shown below). Dye solutions were simply carefully placed on top of preformed collagen gels and allowed to diffuse through gels overnight.

recovery half-time between control and gels with 3 × 10^{10} rods/mL but did show that some molecules became part of an immobile fraction in the collagen/AuNR gels (Figure S11).

DISCUSSION

Many studies examine the effects of nanomaterials on cellular processes; here, we add in the key component of the extracellular matrix to the nanomaterial/cell system. Rather than focusing on what dose of nanomaterials kills cells, we focus on how cellular behavior is altered upon nanomaterial exposure at relatively modest levels.

We have already shown, in previous work, that different polyelectrolytes on gold nanorods alter collagen's mechanical properties, with the high local concentration of charge a key parameter.[42] As cells respond to mechanical cues as well as chemical cues, it was reasonable to expect that cellular behavior would be altered in the presence of nanomaterial-induced altered extracellular matrix. The question, then, becomes can we disentangle mechanical effects from chemical effects in the nanomaterial-ECM-cell system?

In the present work, we have shown that negatively charged AuNRs can induce spontaneous migration of MDA-MB-231 metastatic cancer cells from one area to another as a function of AuNR concentration in 3D ECM mimics. This result is in contrast to earlier reports of 2D migration inhibition by gold NPs,[22,23] and highlights the importance of the ECM and, possibly, cell type, in determining the real *in vivo* effect NPs could have. We note that in our own laboratory we have found that different cell types (PC3 and HDF cells) migrate faster or slower in 2D upon gold nanoparticle exposure, depending on nanoparticle type and cell type.[21] In this study, metastatic MDA-MB-231 cancer cells were used in 3D environments; and we find that these cells migrate *more* to gold nanorod-containing 3D environments. The ability of AuNRs in the ECM to promote enhanced spontaneous migration of metastatic cancer cells could have important implications in the use of NPs at various stages of cancer treatment; NPs in the human body, used as delivery vehicles or as therapeutics,[1−3,8,9] could have unintended side effects that need to be carefully understood. While type I collagen as a model ECM is good start for studying the effect of nanomaterials in ECM, in reality, the ECM of living tissues is a complex, dynamic combination of structural proteins including various types of collagen, fibronectin, elastin and laminin and proteoglycans.[52] In our experiments, AuNRs were added to the ECM during new collagen polymerization and not to pre-existing collagen networks. Cancers (especially breast cancers) are often accompanied by the drastic enhancement of new type I collagen production by stromal cells and fibrosis.[39,53−55] Therefore, our experiments are simple models of how metastatic cancer cells respond when they come upon a 3D extracellular matrix that contains nanomaterials. The general result that nanomaterial-ECM matrices promotes cancer cell migration is, therefore, a cause for concern.

We developed two hypotheses of the mechanism(s) behind the enhanced cell migration in these collagen/AuNR matrices: (i) AuNRs could change the mechanical and structural properties of the collagen gel networks, leading to predictable cellular changes, and/or (ii) AuNRs, known for adsorbing proteins and molecules from media,[17−19,25] alter biochemical gradients and molecular diffusion that then lead to less-predictable changes in cellular behavior. However, these hypotheses are not mutually exclusive; both processes can occur during the course of the experiment. Ultimately, we find some evidence for both mechanisms.

The primary result (Figure 2) shows that more metastatic cancer cells moved from a 3D inner gel to an AuNR-containing outer gel as a function of AuNR concentration. Rheological measurements comparing gels with and without AuNR incorporation showed that gels became stiffer and more elastic with AuNRs, but that this effect was not measurably dependent on AuNR concentration. Additionally, fibrillogenesis lag time was decreased; collagen polymerizes into fibrils made of cross-linked staggered arrays of individual

collagen triple-helix molecules.[56] This indicates that the AuNRs may promote fibril nucleation, most likely *via* an electrostatic interaction between the slightly positive collagen monomers and the negatively charged PSS-coated AuNRs.[42,57] This effect was measured previously and was shown to occur with other negatively charged AuNRs, but not positively charged ones.[42] Complementary microscopic studies revealed structural changes such as increased individual fibril frequency, rigidity and density, and decreased porosity. AuNRs were often found to be accumulated inside of large collagen aggregations that disrupted the collagen networks; this is consistent with the negatively charged AuNRs acting as nucleation sites for fibril formation. Finally, dye diffusion studies indicated that positively charged molecular diffusion is altered in collagen/AuNR gels compared to collagen gels alone. The ability of the AuNR-containing collagen to stop the diffusion of some molecules means that potentially the soluble milieu that cells experience is altered in these gels, as we have observed in previous work.[25] Overall, AuNRs influence both the microstructure/mechanical properties and biochemical diffusion in self-assembled type I collagen gels in ways that could contribute to enhanced spontaneous cell migration.

Mechanotransduction pathways allow for cells to "feel" and respond to mechanical cues from the outer gel even when inside the inner gel. It is most likely the mechanical property and architectural changes that are driving the cells to move toward the outer gel initially.[35−37,58−61] The movement of cells toward stiffer, less porous gels is consistent with the phenomenon of durotaxis, where cells tend to move along a stiffness gradient toward the stiffer region.[58−61] It is unclear from these studies whether the cells migrating from the inner gel to the outer gel experience a stiffness gradient at the interface. Stiffness of self-assembled fibrous materials like type I collagen is intrinsically related to the porosity: as pore size decreases, stiffness increases. It has been reported that human foreskin fibroblasts showed decreased collagen translocation but increased migration in stiffer, less porous collagen gels.[62] However, the relationship between stiffness and migration may not be as simple in 3D; DU-145 human prostate carcinoma cells were found to migrate toward softer ECM when ligand density and integrin receptor levels were held constant.[63]

While it seems that cells migrating more toward a stiffer substrate than a softer one is congruent with durotaxis, durotaxis is thought to be a result of differences in focal adhesion strength and lifetime, and increased polarization.[58−61,64,65] This is contrary to results of characterization of the migratory phenotype of the cells in collagen/AuNR gels, where there is some evidence of an emerging amoeboid-like phenotype. Cells migrating through AuNR-containing type I collagen exhibited rounded locomotion compared to the cyclic elongated motion of control cells, and migrated in a much more random and undirected fashion. Mesenchymal-amoeboid transitions are often distinguished by induction of this rounded nature of motion, reduced cellular adhesion and integrin clustering, and lack of protease activity.[45−50] We found that β1-integrin expression and clustering were significantly decreased in cells migrating in collagen/AuNR gels compared to controls, and that overall cellular adhesion was greatly decreased to collagen/AuNR gels relative to collagen gels.

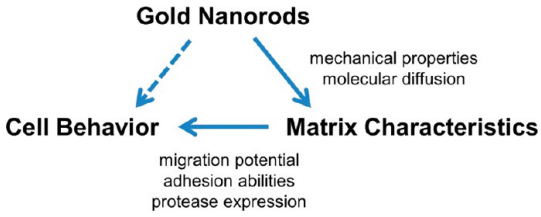

Figure 11. Schematic depicting how gold nanorods alter matrix characteristics, which in turn alter cell behavior. Thus, gold nanorods indirectly affect cell behavior when incorporated into the structural environment.

It is well-known that cells respond chemically to both mechanical and biochemical cues and that this can result in changes in gene expression of related genes.[35−37,66] The migratory cells produced increased levels of MMPs, which is the opposite of what is expected of amoeboid-like cells.[45−50] No evidence of alterations to the Rho-ROCK pathway were detected either, opposite to what is expected for a cellular transition to an amoeboid type. Furthermore, the amoeboid migration mode is associated with highly porous, soft matrices that cells can easily deform,[45−50,67] but due to the decreased porosity of the gels with AuNRs, MMPs are still required for movement regardless of locomotion strategy. These results do not exclude these cells from being categorized as amoeboid-like as there is not a simple dichotomy between mesenchymal and amoeboid-like cells but rather a continuum.[45−50,67] Mesenchymal-amoeboid switches are most often induced in MDA-MB-231 cells by blocking proteolysis, but it is well-known that the transitions can also be induced by reducing the cell-matrix adhesion capability.[47,67−69]

Overall, we propose the following scheme (Figure 11):

1. Cells in a cell-rich 3D environment migrate out more to a 3D environment containing AuNRs due, initially, to the altered mechanical nature of the matrix that is due to the physical presence of the AuNRs (ECM stiffer, more dense, more elastic, shorter fibrils, dye diffusion experiments, *etc.*).
2. Upon crossing to the outer gel, the local chemical environment of the cells is altered due to matrix molecule adsorption to AuNRs (*cf.* dye diffusion experiments); the larger the

concentration of AuNRs, the more the local concentrations are affected. This might explain the concentration dependence of the migration.

3. Upon encountering ECM containing AuNRs, the cells become more rounded, exhibit reduced integrin expression, increased MMP expression, and no changes in RhoA/ROCK1/Rac1 expression. These somewhat contradictory data may be the result of both mechanical changes and biochemical changes in the cellular environment.
4. If "forced" to uptake AuNRs directly, no changes in cellular migration are observed compared to controls, suggesting that direct intracellular effects of the nanomaterials on the actin network are not the primary cause of the inner gel/outer gel migration data (unlike what we have observed before with smaller gold nanoparticles in different cell lines, where the internal actin network can be disrupted).[70]

CONCLUSIONS

We have shown that there is a complex effect of AuNRs in the ECM on MDA-MB-231 cancer cell migration induced by multiple possible factors. AuNRs alter the mechanical properties and the structure of collagen matrices, hinder the diffusion of some molecules and reduce cellular adhesion. Inconsistencies between the increased stiffness and decreased porosity, and decreased adhesion and amoeboid-like cell movement indicate that while changes to the physical properties of the collagen may induce migration to the outer gel, reduced adhesion due to the AuNRs at the interface and beyond may be the origin of the emergence of the amoeboid-like phenotype. Overall, the AuNRs were shown to alter matrix characteristics, which in turn led to altered cell migration, adhesion and protease expression (Figure 11). The stark contrast between the results of this study on AuNRs 3D cancer cell migration and results based on 2D migration stresses the importance of the ECM in the analysis of nanomaterials *in vitro*.[21−23] Control of the ECM and cell-matrix interactions is vital for improving our ability to understand and treat various human diseases, such as cancer, heart, liver, renal, central nervous system and lung disease, and just about any type of organ fibrosis.[69,71−74] In this aspect, improved understanding of the effect AuNRs have on the ECM and cell−ECM interactions could be exploited to gain further control over ECM and biomaterial properties with a new, multidimensional approach.

MATERIALS AND METHODS

Materials. Gold(III) chloride trihydrate ($HAuCl_4 \cdot 3H_2O$, ≥99.9%), sodium borohydride ($NaBH_4$), hexadecyltrimethylammonium bromide (CTAB, BioUltra), poly(sodium-4-styrenesulfonate) (PSS, M.W. 70 000 g/mol), and poly(diallyldimethylammonium chloride) (PDADMAC, very low molecular weight) were all purchased from Aldrich and used as received. PureCol type I bovine collagen solution (3 mg/mL) was purchased from Advanced BioMatrix. 4-(2-hydroxyethyl)-1-piperazineethanesulfonic acid (HEPES) was purchased from Research Products International and 10X minimal essential medium (MEM) was purchased from Sigma. MDA-MB-231 cells (ATCC HTB-26) were obtained frozen from ATCC. Cell culture medium contained Dulbecco's modified eagle medium (DMEM, without phenol red), nonessential amino acids and penicillin-streptomycin solution from Mediatech, and fetal bovine serum (FBS) from Gemini Bio-Products. Medium contained 2.5 μg/mL Fungizone antimycotic (Gibco) when AuNRs were added. All solutions were made with ultrapure deionized water (18.2 MΩ, Barnstead NANOpure II) and all glassware was cleaned with aqua regia prior to use for AuNR synthesis. All cell culture and experiments were done in a sterile environment using typical sterile techniques. Brightfield time-lapse microscopy was done on a Zeiss Axio Observer Z1 inverted compound microscope (with incubation chamber, heated stage and CO_2 sensor) and confocal fluorescence microscopy, confocal reflectance microscopy and fluorescence recovery after photobleaching (FRAP) measurements were performed on a Zeiss 710 multiphoton confocal microscope. Transmission electron microscopy (TEM) was done on a 2100 JEOL Cryo TEM and scanning electron microscopy (SEM) was done on a Hitachi 4700 SEM. Rheological measurements were collected on a TA Instruments AR-G2 rheometer. Absorption spectra of RNA were collected with a Nanodrop 1000 instrument. qPCR was done on the 7900HT Fast Real-Time PCR System (Applied Biosystems) with corresponding Sequence Detection Systems software (Applied Biosystems).

Synthesis and Preparation of Gold Nanorods. Aspect ratio 18 AuNRs were synthesized *via* a scaled-up version of our seed-mediated three-step approach, as previously described.[75,76] ~4 nm diameter gold seeds were made first by reduction of 250 μm aqueous $HAuCl_4$ in 0.1 M CTAB with 0.01 M $NaBH_4$. This solution was stirred (~10 min) and used in a three-step growth procedure after 5 h. For the three-step growth procedure, three growth solutions of 0.1 M CTAB, 250 μM $HAuCl_4$, and 500 μM ascorbic acid were prepared, with the first two solutions containing a final volume of about 36 mL and the final solution containing about 360 mL in a glass flask. Four mL of the gold seed solution was transferred to the first growth solution, and after 15 s, 4 mL of this first solution was transferred to the second growth solution. After another 30 s, the entire second solution was transferred to the final growth solution. This was allowed to sit overnight before pouring off the supernatant and rinsing the AuNRs off the bottom of the flask with water. These nanorods were washed by centrifugation (3500 rcf, 10 min) twice and autoclaved (for use in cell culture experiments) before being concentrated and coated with polyelectrolytes.

Layer-by-layer (LbL) deposition of polyelectrolytes onto the CTAB-coated AuNRs was done as previously described,[77] but under sterile conditions in order to keep AuNRs free of contamination before use with cell studies. All solutions used for LbL coating were made in autoclaved 18MΩ/cm water in sterile containers. The success of each wrapping step was verified by a ZetaPALS zeta potential analyzer (Brookhaven Instruments Corporation). Briefly, the positively charged as-prepared AuNRs were shaken in 1 mL of 1 mM NaCl and 200 μL of 10 mg/mL PSS for approximately 1 h. The polymer was removed by centrifugation at 3500 rcf for 10 min and the newly negatively charged AuNRs were again shaken in 1 mL of 1 mM NaCl, this time with 200 μL of 10 mg/mL PDADMAC. After centrifugation, again the AuNRs were put into the PSS wrapping solution for 1 h and centrifuged. The pellet was finally redispersed into sterile water and the concentration was determined by the absorbance at the transverse peak by UV−vis spectroscopy with a Cary 500 Scan UV−vis−NIR spectrophotometer (Varian).

3D Migration Assay. MDA-MB-231 cells were grown to confluency in cell culture flasks and used before passage 10. Cells

were detached with trypsin/EDTA and resuspended in freshly prepared 1:1:8 (v/v/v) of 10X MEM:2 M HEPES (pH 9.0):collagen solution to a cell concentration of 200 000 cells/mL. The light pink cell/collagen solution was then pipetted in 100 μL aliquots into the wells of a 96-well plate. These "inner gels" were incubated at 37 °C and 5% CO_2 to polymerize for at least 1 h before adding medium. The medium was added while detaching the gels from the wells by injecting the medium under the gels with a syringe. After adding the medium, the gels were placed back into the incubator overnight. The next day, AuNRs were transferred into microcentrifuge tubes and centrifuged at 3500 rcf for 10 min. The supernatant was removed and the pellet was redispersed in 10X MEM and HEPES solutions, followed by collagen solution to make the final 1:1:8 collagen solution. AuNRs were added just prior to polymerization in order to get enough AuNRs into the sample. Samples were made with AuNR concentrations varying between zero and 3×10^{10} rods/mL collagen solution (1×10^9 rods/mL = ~1.7 pM, 5×10^9 rods/mL = ~8.3 pM, 1×10^{10} rods/mL = ~17 pM, 2×10^{10} rods/mL = ~33 pM, 3×10^{10} rods/mL = ~50 pM). This collagen/AuNR solution was used to mold into "outer gels" to encapsulate the previously made cell-containing "inner gels". To do this, 150 μL of the collagen/AuNR solution was added to coat the bottom of one well of an 8-well chamber slide. Then, using a syringe, one "inner gel" was transferred on top of this aliquot, followed by a second 150 μL of the collagen/AuNR solution to embed the "inner gel". The "outer gel" was then allowed to polymerize for at least 1 h at 37 °C and 5% CO_2 before adding a small volume of complete medium (with 10% FBS) on top of each gel construct. The gels were then incubated for 4 days to allow for cell migration before imaging. The medium on top of the gels was changed daily to keep the cells healthy; some nanorod loss in the washings was observed. Images were taken all around the perimeter of the inner gel, wherever any cells had moved across the interface. "AuNR-treated" control samples were made by replacing untreated cells with cells that had been exposed to 3×10^{10} rods/mL in 10 mL media in the culture flask for 24 h before being trypsinized and suspended in freshly prepared 1:1:8 (v/v/v) of 10X MEM:2 M HEPES (pH 9.0): collagen solution to a cell concentration of 200 000 cells/mL. "Antibody-treated" control samples were made with cells that had been pretreated with 10 μg/mL P5D2 anti-β1-integrin blocking antibody for 15 min at 37 °C and 5% CO_2 prior to encapsulation in collagen solution. "PSS control" samples were made with untreated cells encapsulated in 1:1:8 (v/v/v) of 10X MEM:2 M HEPES (pH 9.0):collagen solution with the addition of 0.1 mg/mL PSS. PSS was dissolved in the 10X MEM solution prior to incorporation into the collagen solution. 0.1 mg/mL is excess of a rough estimate of the concentration of PSS in the 3×10^{10} rods/mL gels, assuming a 3.0 nM coating,[75] and using the powder density of PSS and the average dimensions of the AuNRs.

Nanorod Uptake and Toxicity Analysis. The toxicity of the collagen/AuNR gels was determined using a MarkerGene Live: Dead/Cytotoxicity Assay Kit. 200 000 cells/mL were cultured in 1:1:8 (v/v/v) 10X MEM:2 M HEPES (pH 9.0):collagen solution or collagen solution containing between 1×10^9 and 3×10^{10} rods/mL gel for 24 h with medium in 8-well chamber slides. The gels were transferred to a 24-well plate and washed several times for 15 m increments in 1X phosphate buffered saline (PBS) before being stained for 1 h with a working solution of 2 μM carboxyfluorescein diacetate and 4 μM propidium iodide (PBS) from the kit. Gels were washed several times with 1X PBS and imaged by fluorescence microscopy. Three separate gels were imaged for each sample type in ten random spots per gel (>1000 cells per AuNR concentration).

Nanorod uptake was visualized by first culturing 200 000 cells/mL in 3×10^{10} rods/mL 1:1:8 (v/v/v) 10X MEM:2 M HEPES (pH 9.0):collagen for 4 days with medium in 8-well chamber slides. Gels were then scooped into a type I collagenase (Invitrogen) solution (1000 units/mL medium) for 30 min at 37 °C. After all collagen was dissolved, cells were washed in medium three times to remove nonendocytosed AuNRs, before plating 30 000 cells into a 35 mm well glass-bottomed culture dish (MatTek Corporation). After allowing cells to adhere for 1 h, any additional AuNRs not inside cells were washed away by five washes with medium. Samples were then fixed for 15 min with 4% prewarmed paraformaldehyde (in PBS), permeabilized for 10 min with 0.5% Triton X-100 (Sigma, BioUltra) and stained with 1:100 fluorescein phalloidin (Molecular Probes, F-actin stain) for 1 h and 300 nM 4′,6-diamidino-2-phenylidole dihydrochloride (DAPI, Molecular Probes, nuclei stain) for 30 min. Completed samples were imaged by confocal fluorescence microscopy and the AuNRs were visualized by their reflectance signal with a 488 nm argon laser. Inductively coupled plasma mass spectrometry (ICP-MS) studies were attempted for quantification of AuNR uptake, but were unsuccessful with extremely large variation between samples as a result of variable separation of cell-bound nanorods and gel-bound nanorods. We believe that this is because it is difficult to separate nonendocytosed AuNRs of this size and surface coating from the cells by centrifugation; the AuNRs aggregate after collagenase treatment and easily sediment on their own and cannot be reliably separated from the cells. Therefore, as an alternate to AuNR uptake quantification by ICP-MS, a set of experiments were done in which cells were directly incubated with extremely large quantities of AuNRs, and these "AuNR-treated" cells were then subject to the inner gel/outer gel migration experiments (Figure 2).

Rheology of Collagen/AuNR Gels. All components of the collagen solution were kept on ice and the 1:1:8 (v/v/v) 10X MEM:2 M HEPES (pH 9.0):collagen solutions were prepared immediately before individual rheology measurements. Each sample was loaded into a parallel plate geometry (40 mm top plate with solvent trap) with a 500 μm gap with the temperature-controlled bottom plate set to room temperature. The edge of the sample was coated with mineral oil and the solvent trap filled with water to prevent dehydration. The temperature of the bottom plate was then raised to 37 °C and the samples were allowed to polymerize between the plates for 30 min while monitored under sinusoidal shear strain at 2 rad/s and 1% strain. After 30 min polymerization, the sample was subjected to a frequency sweep between 0.1 to 10 Hz at 1% strain (linear viscoelastic region verified with amplitude sweep). Three samples were run for each of the six tested AuNR concentrations.

Microscopy of Collagen/AuNR Gels. Gels were imaged by various methods. For confocal reflectance imaging, 200 μL freshly prepared 1:1:8 (v/v/v) 10X MEM:2 M HEPES (pH 9.0):collagen solution (with various AuNR concentrations) was placed on top of a clean glass coverslip and covered by another coverslip. These samples were incubated at 37 °C for at least 1 h before imaging. Three samples were made for each AuNR concentration and Z-stack image sets were collected with a 63× oil objective in five random spots per sample from ~50 μm above the bottom coverslips for 80 slices of ~0.40 μm thickness (total range of 31.43 μm). The reflectance signal of a 488 nm argon laser was collected.

Gels for scanning electron microscopy (SEM) were prepared by two separate methods. In the first method, 1:1:8 (v/v/v) 10X MEM:2 M HEPES (pH 9.0):collagen solution (with or without AuNRs) was pipetted onto clean glass coverslips and allowed to polymerize at 37 °C for 1 h. The samples were then fixed with 2% aq. glutaraldehyde overnight, followed by four 15 min washes with deionized water. Samples were dehydrated by stepwise ethanol addition (30, 50, 70, 85, 100% ethanol) followed by CO_2 supercritical drying, SEM sample mounting and sputter coating with Au/Pd. SEM samples were also prepared by a second method in which they were first fixed with Karnovsky's fixative in a microcentrifuge tube, washed with Sorenson's buffer, fixed with osmium tetroxide and dehydrated by stepwise ethanol addition. The samples were then mixed with 1:1 ethanol and hexamethyldisilazane (HMDS), then incubated in pure HMDS and dried, SEM sample mounted and sputter coated with Au/Pd. Samples were gently centrifuged between steps. Dried samples were stored under a vacuum.

Samples for transmission electron microscopy (TEM) were prepared much like the second type of SEM sample. 1:1:8 (v/v/v) 10X MEM:2 M HEPES (pH 9.0):collagen samples (with or without AuNRs) were polymerized in microcentrifuge tubes and fixed with Karnovsky's fixative, followed by washing with Sorenson's

buffer and fixing with osmium tetroxide (potassium ferrocyanide added 10 min before end of incubation). The samples were then washed, dehydrated by stepwise ethanol addition and transitioned to epoxy using acetonitrile. After allowing the sample to harden in pure epoxy at 70 °C overnight, the microcentrifuge tube was removed and the end was clipped and reset on an epoxy stub. Finally, after rehardening, the sample blocks were cut with a diamond knife and left unstained.

Dye Diffusion Experiments. For the visible dye diffusion experiments, 1:1:8 (v/v/v) 10X MEM:2 M HEPES (pH 9.0):collagen gels were prepared by molding 3 mL of collagen solution (without AuNRs or with 3×10^{10} rods/mL) into glass vials and incubating at 37 °C overnight. Aqueous 1 mM Methylene Blue (Sigma) or 1 mM Remazol Brilliant Blue R (Sigma) were carefully pipetted on top of the gels at a fixed volume. The dyes were allowed to diffuse through untouched overnight.

For fluorescein fluorescence recovery after photobleaching (FRAP), 1:1:8 (v/v/v) 10X MEM:2 M HEPES (pH 9.0):collagen gels were prepared in 8-well chamber slides and allowed to gel overnight at 37 °C. The gels were then transferred to a 24-well plate and incubated in 3 mg/mL aq. sodium fluorescein (Acros Organics) for 8 h. Samples were transferred to glass-bottomed culture dishes immediately before FRAP experiment, covered with remaining fluorescein solution and covered with a No. 1 glass coverslip. FRAP was done ~50 μm from the bottom of the sample with a 70 nm circular region of interest. Bleaching was started after ten 1 s scans (out of a total of 200 1 s scans) with a 488 nm argon laser at 100% power (25.0 mW) for 800 iterations. When not bleaching, scans were collected with the 488 nm laser at 0.09% power.

Confocal Fluorescence Microscopy of Cells. Live cells cultured in 1:1:8 (v/v/v) 10X MEM:2 M HEPES (pH 9.0):collagen collagen gels were stained for F-actin and nuclei for analysis of cell morphology. Cells were first cultured at 200 000 cells/mL in collagen without AuNRs or with 3×10^{10} rods/mL collagen for 4 days in 8-well chamber slides. Gels were fixed with 4% prewarmed paraformaldehyde (in PBS) for 1 h at RT and then transferred to a 24-well plate. Long (5−15 min) washing steps in PBS were done multiple times between each step. Gels were permeabilized for 10 min with 0.5% Triton X-100, blocked with 1% bovine serum albumin (BSA, ChemCruz) and 10% FBS for 1 h, and stained with 100 nM rhodamine phalloidin (Cytoskeleton, Inc.) for 90 m and 300 nM DAPI for 30 min before being stored in PBS at 4 °C. Samples were imaged with confocal fluorescence microscopy.

Cells were also stained for β1-integrin expression inside the 1:1:8 (v/v/v) 10X MEM:2 M HEPES (pH 9.0):collagen or collagen/AuNR gels. For this, 4-day old gels were fixed overnight with 4% prewarmed paraformaldehyde (in PBS) at RT, followed by a blocking/permeabilization step with 1% BSA, 10% FBS and 0.5% Triton X-100 overnight at RT. Gels were washed at least three times with PBS for 5 min between the remaining steps. Anti-β1-integrin blocking antibody, clone P5D2 (mouse monoclonal, EMD Millipore) was added to the samples at 2 μg/mL in PBS with 1% BSA and 0.3% Triton X-100 for 24 h. 1:100 goat antimouse Alexa Fluor 488-conjugate secondary antibody (EMD Millipore) was then added for 4 h at RT, followed by 300 nM DAPI for 30 min at RT. Samples were then imaged with confocal fluorescence microscopy. AuNR-treated cells were also tested as controls exactly the same way, but cells were exposed to 3×10^{10} rods/mL in 10 mL of media for 24 h in a culture flask before being recast into collagen gels.

Brightfield and Time-Lapse Microscopy of Cells. Brightfield micrographs were collected with transmitted light through a 10× objective. Live cells in 1:1:8 (v/v/v) 10X MEM:2 M HEPES (pH 9.0): collagen (with or without AuNRs) were imaged under incubation conditions (37 °C, 5% CO_2) with medium. Antibody-treated cells pretreated with 10 μg/mL P5D2 anti-β1-integrin blocking antibody for 15 min at 37 °C and 5% CO_2 and AuNR-treated cells exposed to 3×10^{10} rods/mL in 10 mL of media for 24 h in a culture flask were also imaged in collagen. Only migrated cells (cells that were in the outer gel) were counted in morphology studies. For time-lapse studies, images were taken every 10 min for 24 h of live cells under incubation conditions.

Cell-Matrix Adhesion Assays. Cell-matrix adhesion assays were done in 96-well plates, and as described by Kucik and Wu.[51] The wells were first coated with 100 μL 1:1:8 (v/v/v) 10X MEM:2 M HEPES (pH 9.0):collagen solution (some without AuNRs, some with 3×10^{10} rods/mL as designated by sample type) overnight at 37 °C and 5% CO_2. The wells were then blocked with heat-denatured 10 mg/mL BSA in PBS for 1 h at 37 °C and 5% CO_2. The wells were then washed twice with PBS and 100 μL of 3×10^{10} rods/mL PBS were added to the collagen/AuNR-coated wells ("collagen/rods + rods", 100 μL PBS was added to all others) for 1 h at 37 °C and 5% CO_2. The wells were washed twice more with PBS and 100 μL of 400 000 cells/mL medium was added to each sample well for 2 h at 37 °C and 5% CO_2 (not including blanks, to which 100 μL of medium was added instead). For control samples ("collagen + cells"), cells were added to wells coated with MEM/HEPES/collagen solution. For 3×10^{10} rods/mL samples ("collagen/rods + cells") cells were added to wells coated with MEM/HEPES/collagen containing 3×10^{10} rods/mL. For antibody-treated samples ("collagen + antibody-treated cells"), cells were incubated in medium with 10 μg/mL P5D2 anti-β1-integrin blocking antibody for 15 min at 37 °C and 5% CO_2 before adding to wells coated with MEM/HEPES/collagen solution (no AuNRs). For nanorod-treated samples ("collagen + nanorod-treated cells"), 3×10^{10} rods/mL medium was added to the cells in the culture flask for 24 h before trypsinizing and adding to wells coated with MEM/HEPES/collagen solution (no AuNRs). After incubation with cells, wells were washed twice with PBS and 60 μL of substrate solution (3.75 mM *p*-nitro-pheno-*N*-β-D-glucosaminide, 50 mM citrate, pH 5.0) were added to each well and incubated at 37 °C and 5% CO_2 for 90 min. Finally, 90 μL of stop buffer (5 mM EDTA, 50 mM glycine, pH 10.4) was added to each well, and the plate was read at 405 nm. Because of the optical absorbance of both AuNRs and collagen solutions, proper blanks (no cells) were made with just MEM/HEPES/collagen, AuNRs/collagen and AuNRs/collagen with additional rods added on top.

Quantitative Real-Time Polymerase Chain Reaction (qPCR). In order to analyze the relative expression of matrix metalloproteinase (MMPs), quantitative real-time polymerase chain reaction (qPCR) analysis was performed. For control samples and samples with 3×10^{10} rods/mL collagen, cells were cultured at 200 000 cells/mL in MEM/HEPES/collagen with the appropriate amount of AuNRs (control contained no AuNRs). For antibody-treated samples, cells were first incubated with 10 μg/mL P5D2 anti-β1-integrin blocking antibody in 10X MEM for 15 min at 37 °C and 5% CO_2 before adding the HEPES and collagen product solution to 200 000 cells/mL. For nanorod-treated samples, cells were first allowed to uptake AuNRs from medium (3×10^{10} rods/mL medium) for 24 h in a cell culture flask before being trypsinized and cultured in the collagen solution at 200 000 cells/mL. After 4 days culture, samples were removed from collagen with a 1000 unit/mL collagenase solution (in medium) at 37 °C and 5% CO_2. The cells were washed in medium once and then left as a pellet. Total RNA was extracted and purified per manufacturer's protocols using an RNeasy Midi kit (Qiagen). Briefly, Buffer RLT was added to the cell pellet and cells were homogenized by rapid mixing and vortexing. 70% ethanol was mixed in and the lysate solution was added to the RNeasy spin column and centrifuged at 4000 rcf for 5 min. Flow-through was discarded and centrifugation and flow-through steps were repeated with Buffer RW1 and twice with Buffer RPE. RNA was finally eluted with RNase-free water and tested for concentration and quality by absorbance readings (stored at −80 °C until ready to dilute and use). For each sample type, RNA was collected and processed separately for three separate samples and each of these samples was analyzed in duplicates in the final PCR assay.

The PCR reaction was done using the AgPath-ID one-step RT-PCR kit (Applied Biosystems), as previously described.[78] Reverse transcription and amplification of 2 μL of 25 ng/μL purified RNA was done in a 10 μL reaction mixture containing 5 μL of 2X RT-PCR buffer, 0.4 μL of 25X RT-PCR enzyme mix,1.25 μL yeast RNA (5 mg/mL, Ambion) and 0.5 μL TaqMan gene-specific primer/probe sets (Applied Biosystems). The primer/probe sets (FAM labels) used were as follows: MMP1, Hs00899658_m1; MMP2, Hs01548727_m1; MMP9, Hs00234579_m1; MMP13, Hs00233992_m1 and MMP14, Hs01037009_g1. Three reference

genes, GADPH (Hs99999905_m1), B2M (Hs_99999907_m1) and HPRT1 (Hs99999909_m1) were analyzed as well, but only HPRT1 ended up being suitable as a reference gene for this cell type. mRNA of the probed genes was quantified by qPCR (10 min at 45 °C, 10 min at 95 °C and then 40 cycles of 15 s at 95 °C and 45 s at 65 °C). Nontemplate controls were used as controls for each primer/probe set. Relative expression levels were calculated after normalization against the HPRT1 reference gene. Statistical analysis of the qPCR data was performed using the web-based RT^2 Profiler PCR Array Data Analysis software (SABiosciences, www.SABiosciences.com/pcrarraydataanalysis.php). This software transforms C_t values to fold changes using the $\Delta\Delta C_t$ method with normalization to the reference/housekeeping gene *via* geometric mean.

Conflict of Interest: The authors declare no competing financial interest.

Supporting Information Available: Live/dead analysis results for cells in collagen for all AuNR concentrations used throughout study, confocal fluorescence micrographs of MDA-MB-231 cells with endocytosed AuNRs, comparison of live/dead results *versus* controls for each AuNR concentration tested with additional antibody-treated, AuNR-treated and PSS control cell samples, elongation factor data for all sample types and controls tested, movies depicting the movement of cells under all conditions tested, confocal fluorescence micrographs of AuNR-treated cells migrating through collagen, average raw threshold cycle values, fold change values *versus* average cycle value per sample and fold regulation values for qPCR results, full averaged frequency sweep graphs showing storage and loss moduli (Pa) *versus* frequency (Hz) for all sample types, averaged tan(δ) values from rheology at 1 Hz for all sample types, 3D reconstructed Z-stack confocal reflectance microscopy images for collagen/AuNRs at all concentrations, grayscale pixel value *versus* pixel count for quantification of collagen reflectance signal for each sample type, mobile fraction and recovery half-time plots for FRAP with fluorescein in collagen and collagen/AuNR samples. The Supporting Information is available free of charge on the ACS Publications website at DOI: 10.1021/acsnano.5b03362.

Acknowledgment. This work is supported by the National Science Foundation (CHE-1011980 and CHE-1306596). E.M.G. was funded at UIUC from NIH National Cancer Institute Alliance for Nanotechnology in Cancer 'Midwest Cancer Nanotechnology Training Center' Grant R25 CA154015A and thanks UIUC for the James R. Beck Fellowship and the Harry S. Drickamer Fellowship. TEM and SEM studies were carried out in the Frederick Seitz Materials Research Laboratory Central Research Facilities (UIUC), and we thank Lou Ann Miller of the Biological Electron Microscopy center for assistance with collagen TEM and SEM samples. Confocal fluorescence microscopy was done within the Core Facilities at the Institute for Genomic Biology (UIUC). We thank the Randy Ewoldt group (UIUC) for assistance and use of their rheometer and the Cell Media Facility (UIUC) for help with cell cultures, and Professor Edie Goldsmith for helpful discussions. E.M.G. and C.J.M. conceived and planned the study. E.M.G. performed experiments. E.M.G. and C.J.M. wrote the manuscript.

REFERENCES AND NOTES

1. Dreaden, E. C.; Alkilany, A. M.; Huang, X.; Murphy, C. J.; El-Sayed, M. A. The Golden Age: Gold Nanoparticles for Biomedicine. *Chem. Soc. Rev.* **2012**, *41*, 2740–2779.
2. Giljohann, D. A.; Seferos, D. S.; Daniel, W. L.; Massich, M. D.; Patel, P. C.; Mirkin, C. A. Gold Nanoparticles for Biology and Medicine. *Angew. Chem., Int. Ed.* **2010**, *49*, 3280–3294.
3. Lohse, S. E.; Murphy, C. J. Applications of Colloidal Inorganic Nanomaterials: From Medicine to Energy. *J. Am. Chem. Soc.* **2012**, *134*, 15607–15620.
4. Leduc, C.; Si, S.; Gautier, J.; Soto-Ribeiro, M.; Wehríe-Haller; Gautreau, A.; Giannone, G.; Cognet, L.; Lounis, B. A Highly Specific Gold Nanoprobe for Live-Cell Single-Molecule Imaging. *Nano Lett.* **2013**, *13*, 1489–1494.
5. Ando, J.; Fujita, K.; Smith, N. I.; Kawata, S. Dynamic SERS Imaging of Cellular Transport Pathways with Endocytosed Gold Nanoparticles. *Nano Lett.* **2011**, *11*, 5344–5348.
6. Murphy, C. J.; Gole, A. M.; Stone, J. W.; Sisco, P. N.; Alkilany, A. M.; Goldsmith, E. C.; Baxter, S. C. Gold Nanoparticles in Biology: Beyond Toxicity to Cellular Imaging. *Acc. Chem. Res.* **2008**, *41*, 1721–1730.
7. Saha, K.; Agasti, S. S.; Kim, C.; Li, X.; Rotello, V. M. Gold Nanoparticles in Chemical and Biological Sensing. *Chem. Rev.* **2012**, *112*, 2739–2779.
8. Alkilany, A. M.; Thompson, L. B.; Boulos, S. P.; Sisco, P. N.; Murphy, C. J. Gold Nanorods: Their Potential for Photothermal Therapeutics and Drug Delivery, Tempered by the Complexity of their Biological Interactions. *Adv. Drug Delivery Rev.* **2012**, *64*, 190–199.
9. Ghosh, P.; Han, G.; De, M.; Kim, C. K.; Rotello, V. M. Gold Nanoparticles in Delivery Applications. *Adv. Drug Delivery Rev.* **2008**, *60*, 1307–1315.
10. Sperling, R. A.; Parak, W. J. Surface Modification, Functionalization and Bioconjugation of Colloidal Inorganic Nanoparticles. *Philos. Trans. R. Soc., A* **2010**, *368*, 1333–1383.
11. Lohse, S. E.; Eller, J. R.; Sivapalan, S. T.; Plews, M. R.; Murphy, C. J. A Simple Benchtop Reactor System for the High-Throughput Synthesis and Functionalization of Gold Nanoparticles with Different Sizes and Shapes. *ACS Nano* **2013**, *7*, 4135–4150.
12. Mout, R.; Moyano, D. F.; Rana, S.; Rotello, V. M. Surface Functionalization of Nanoparticles for Nanomedicine. *Chem. Soc. Rev.* **2012**, *41*, 2539–2544.
13. Nativo, P.; Prior, I. A.; Brust, M. Uptake and Intracellular Fate of Surface-Modified Gold Nanoparticles. *ACS Nano* **2008**, *2*, 1639–1644.
14. Alkilany, A. M.; Murphy, C. J. Toxicity and Cellular Uptake of Gold Nanoparticles: What Have We Learned So Far? *J. Nanopart. Res.* **2010**, *12*, 2313–2333.
15. Dykman, L. A.; Khlebtsov, N. G. Uptake of Engineered Gold Nanoparticles into Mammalian Cells. *Chem. Rev.* **2014**, *114*, 1258–1288.
16. Mahmoudi, M.; Azadmanesh, K.; Shokrgozar, M. A.; Journeay, W. S.; Laurent, S. Effect of Nanoparticles on the Cell Life Cycle. *Chem. Rev.* **2011**, *111*, 3407–3432.
17. Walkey, C. D.; Olsen, J. B.; Song, F.; Liu, R.; Guo, H.; Olsen, D. W. H.; Cohen, Y.; Emili, A.; Chan, W. C. W. Protein Corona Fingerprinting Predicts the Cellular Interaction of Gold and Silver Nanoparticles. *ACS Nano* **2014**, *8*, 2439–2455.
18. Monopoli, M. P.; Walczyk, D.; Campbell, A.; Elia, G.; Lynch, I.; Baldelli Bombelli, F.; Dawson, K. A. Physical-Chemical Aspects of Protein Corona: Relevance to *In Vitro* and *In Vivo* Biological Impacts of Nanoparticles. *J. Am. Chem. Soc.* **2011**, *133*, 2525–2534.
19. Walkey, C. D.; Olsen, J. B.; Guo, H.; Emili, A.; Chan, W. C. W. Nanoparticle Size and Surface Chemistry Determine Serum Protein Adsorption and Macrophage Uptake. *J. Am. Chem. Soc.* **2012**, *134*, 2139–2147.
20. Friedl, P.; Gilmour, D. Collective Cell Migration in Morphogenesis, Regeneration and Cancer. *Nat. Rev. Mol. Cell Biol.* **2009**, *10*, 445–457.
21. Yang, J. A.; Phan, H. T.; Vaidya, S.; Murphy, C. J. Nanovacuums: Nanoparticle Uptake and Differential Cellular Migration on a Carpet of Nanoparticles. *Nano Lett.* **2013**, *13*, 2295–2302.
22. Zhou, T.; Yu, M.; Zhang, B.; Wang, L.; Wu, X.; Zhou, H.; Du, Y.; Hao, J.; Tu, Y.; Chen, C.; Wei, T. Inhibition of Cancer Cell Migration by Gold Nanorods: Molecular Mechanisms and Implications for Cancer Therapy. *Adv. Funct. Mater.* **2014**, *24*, 6922.
23. Tay, C. Y.; Cai, P.; Setyawati, M. I.; Fang, W.; Tan, L. P.; Hong, C. H. L.; Chen, X.; Leong, D. T. Nanoparticles Strengthen Intracellular Tension and Retard Cellular Migration. *Nano Lett.* **2014**, *14*, 83–88.
24. Sisco, P. N.; Wilson, C. G.; Mironova, E.; Baxter, S. C.; Murphy, C. J.; Goldsmith, E. C. The Effect of Gold Nanorods on Cell-Mediated Collagen Remodeling. *Nano Lett.* **2008**, *8*, 3409–3412.
25. Sisco, P. N.; Wilson, C. G.; Chernak, D.; Clark, J. C.; Grzincic, E. M.; Ako-Asare, K.; Goldsmith, E. C.; Murphy, C. J. Adsorption

of Cellular Proteins to Polyelectrolyte-Functionalized Gold Nanorods: A Mechanism for Nanoparticle Regulation of Cell Phenotype? *PLoS One* **2014**, *9*, e86670.
26. Even-Ram, S.; Yamada, K. M. Cell Migration in 3D Matrix. *Curr. Opin. Cell Biol.* **2005**, *17*, 524–532.
27. Brábek, J.; Mierke, C. T.; Rösel, D.; Veselý, P.; Fabry, B. The Role of the Tissue Microenvironment in the Regulation of Cancer Cell Motility and Invasion. *Cell Commun. Signaling* **2010**, *8*, 22.
28. Tozluoğlu, M.; Tournier, A. L.; Jenkins, R. P.; Hooper, S.; Bates, P. A.; Sahai, E. Matrix Geometry Determines Optimal Cancer Cell Migration Strategy and Modulates Response to Interventions. *Nat. Cell Biol.* **2013**, *15*, 751–762.
29. Friedl, P.; Wolf, K. Proteolytic Interstitial Cell Migration: A Five-Step Process. *Cancer Metastasis Rev.* **2009**, *28*, 129–135.
30. Puklin-Faucher, E.; Sheetz, M. P. The Mechanical Integrin Cycle. *J. Cell Sci.* **2009**, *122*, 179–186.
31. Hood, J. D.; Cheresh, D. A. Role of Integrins in Cell Invasion and Migration. *Nat. Rev. Cancer* **2002**, *2*, 91–100.
32. Guzman, A.; Ziperstein, M. J.; Kaufman, L. J. The Effect of Fibrillar Matrix Architecture on Tumor Cell Invasion of Physically Challenging Environments. *Biomaterials* **2014**, *35*, 6954–6963.
33. Baker, B. M.; Chen, C. S. Deconstructing the Third Dimension – How 3D Culture Microenvironments Alter Cellular Cues. *J. Cell Sci.* **2012**, *125*, 3015–3024.
34. Evans, N. D.; Gentleman, E. The Role of Material Structure and Mechanical Properties in Cell-Matrix Interactions. *J. Mater. Chem. B* **2014**, *2*, 2345–2356.
35. Angelini, T. E.; Hannezo, E.; Trepat, X.; Fredberg, J. J.; Weitz, D. A. Cell Migration Driven by Cooperative Substrate Deformation Patterns. *Phys. Rev. Lett.* **2010**, *104*, 168104.
36. DuFort, C. C.; Paszek, M. J.; Weaver, V. M. Balancing Forces: Architectural Control of Mechanotransduction. *Nat. Rev. Mol. Cell Biol.* **2011**, *12*, 308–319.
37. Wang, N.; Tytell, J. D.; Ingber, D. E. Mechanotransduction at a Distance: Mechanically Coupling the Extracellular Matrix with the Nucleus. *Nat. Rev. Mol. Cell Biol.* **2009**, *10*, 75–82.
38. Chung, C. Y.; Funamoto, S.; Firtel, R. A. Signaling Pathways Controlling Cell Polarity and Chemotaxis. *Trends Biochem. Sci.* **2001**, *26*, 557–566.
39. Schedin, P.; Keely, P. J. Mammary Gland ECM Remodeling, Stiffness, and Mechanosignaling in Normal Development and Tumor Progression. *Cold Spring Harbor Perspect. Biol.* **2011**, *3*, a003228.
40. Grinnell, F.; Rocha, L. B.; Iucu, C.; Rhee, S.; Jiang, H. Nested Collagen Matrices: A New Model to Study Migration of Human Fibroblast Populations in Three Dimensions. *Exp. Cell Res.* **2006**, *312*, 86–94.
41. Tibbitt, M. W.; Anseth, K. S. Hydrogels as Extracellular Matrix Mimics for 3D Cell Culture. *Biotechnol. Bioeng.* **2009**, *103*, 655–663.
42. Wilson, C. G.; Sisco, P. N.; Gadala-Maria, F. A.; Murphy, C. J.; Goldsmith, E. C. Polyelectrolyte-Coated Gold Nanorods and Their Interactions with Type I Collagen. *Biomaterials* **2009**, *30*, 5639–5648.
43. Cox, T. R.; Erler, J. T. Remodeling and Homeostasis of the Extracellular Matrix: Implications for Fibrotic Diseases and Cancer. *Dis. Models & Mech.* **2011**, *4*, 165–178.
44. Jokinen, J.; Dadu, E.; Nykvist, P.; Käpylä, J.; White, D. J.; Ivaska, J.; Vehniläinen, P.; Reunanen, H.; Larjava, H.; Häkkinen, L.; *et al.* Integrin-Mediated Cell Adhesion to Type I Collagen Fibrils. *J. Biol. Chem.* **2004**, *279*, 31956–31963.
45. Wolf, K.; Mazo, I.; Leung, H.; Engelke, K.; von Andrian, U. H.; Deryugina, E. I.; Strongin, A. Y.; Bröcker, E.-B.; Friedl, P. Compensation Mechanism in Tumor Cell Migration: Mesenchymal-Amoeboid Transition after Blocking Pericellular Proteolysis. *J. Cell Biol.* **2003**, *160*, 267–277.
46. Petrie, R. J.; Yamada, K. M. At the Leading Edge of Three-Dimensional Cell Migration. *J. Cell Sci.* **2012**, *125*, 5917–5926.
47. Friedl, P.; Wolf, K. Plasticity of Cell Migration: A Multiscale Tuning Model. *J. Cell Biol.* **2010**, *188*, 11–19.
48. Paňková, K.; Rösel, D.; Novotný, M.; Brábek, J. The Molecular Mechanisms of Transition between Mesenchymal and Amoeboid Invasiveness in Tumor Cells. *Cell. Mol. Life Sci.* **2010**, *67*, 63–71.
49. Sahai, E.; Marshall, C. J. Differing Modes of Tumour Cell Invasion Have Distinct Requirements for Rho/ROCK Signalling and Extracellular Proteolysis. *Nat. Cell Biol.* **2003**, *5*, 711–719.
50. Wyckoff, J. B.; Pinner, S. E.; Gschmeissner, S.; Condeelis, J. S.; Sahai, E. ROCK- and Myosin-Dependent Matrix Deformation Enables Protease-Independent Tumor-Cell Invasion *In Vivo*. *Curr. Biol.* **2006**, *16*, 1515–1523.
51. Kucik, D. F.; Wu, C. Cell-Adhesion Assays. In *Methods in Molecular Biology: Cell Migration: Developmental Methods and Protocols*; Guan, J.-L., Ed.; Humana Press Inc.: Totowa, NJ, 2010; Vol. 294, pp 43–54.
52. Frantz, C.; Stewart, K. M.; Weaver, V. M. The Extracellular Matrix at a Glance. *J. Cell Sci.* **2010**, *123*, 4195–4200.
53. Luparello, C. Aspects of Collagen Changes in Breast Cancer. *J. Carcinog. Mutagen.* **2013**, *S13*, 007.
54. Kalluri, R.; Zeisberg, M. Fibroblasts in Cancer. *Nat. Rev. Cancer* **2006**, *6*, 392–401.
55. Egeblad, M.; Rasch, M. G.; Weaver, V. M. Dynamic Interplay Between the Collagen Scaffold and Tumor Evolution. *Curr. Opin. Cell Biol.* **2010**, *22*, 697–706.
56. Shoulders, M. D.; Raines, R. T. Collagen Structure and Stability. *Annu. Rev. Biochem.* **2009**, *78*, 929–958.
57. Li, Y.; Asadi, A.; Monroe, M. R.; Douglas, E. P. pH Effects on Collagen Fibrillogenesis *In Vitro*: Electrostatic Interactions and Phosphate Binding. *Mater. Sci. Eng., C* **2009**, *29*, 1643–1649.
58. Katsumi, A.; Orr, A. W.; Tzima, E.; Schwartz, M. A. Integrins in Mechanotransduction. *J. Biol. Chem.* **2004**, *279*, 12001–12004.
59. Lo, C.-M.; Wang, H.-B.; Dembo, M.; Wang, Y.-L. Cell Movement is Guided by the Rigidity of the Substrate. *Biophys. J.* **2000**, *79*, 144–152.
60. Plotnikov, S. V.; Pasapera, A. M.; Sabass, B.; Waterman, C. M. Force Fluctuations within Focal Adhesions Mediate ECM-Rigidity Sensing to Guide Directed Cell Migration. *Cell* **2012**, *151*, 1513–1527.
61. Raab, M.; Swift, J.; Dingal, P. C. D. P.; Shah, P.; Shin, J.-W.; Discher, D. E. Crawling from Soft to Stiff Matrix Polarizes the Cytoskeleton and Phosphoregulates Myosin-II Heavy Chain. *J. Cell Biol.* **2012**, *199*, 669–683.
62. Miron-Mendoza, M.; Seemann, J.; Grinnell, F. The Differential Regulation of Cell Motile Activity through Matrix Stiffness and Porosity in Three Dimensional Collagen Matrices. *Biomaterials* **2010**, *31*, 6425–6435.
63. Zaman, M. H.; Trapani, L. M.; Sieminski, A. L.; MacKellar, D.; Gong, H.; Kamm, R. D.; Wells, A.; Lauffenburger, D. A.; Matsudaira, P. Migration of Tumor Cells in 3D Matrices is Governed by Matrix Stiffness Along with Cell-Matrix Adhesion and Proteolysis. *Proc. Natl. Acad. Sci. U. S. A.* **2006**, *103*, 10889–10894.
64. Hoffman, B. D.; Grashoff, C.; Schwartz, M. A. Dynamic Molecular Processes Mediate Cellular Mechanotransduction. *Nature* **2011**, *475*, 316–323.
65. Paszek, M. J.; Zahir, N.; Johnson, K. R.; Lakins, J. N.; Rozenberg, G. I.; Gefen, A.; Reinhart-King, C. A.; Margulies, S. S.; Dembo, M.; *et al.* Tensional Homeostasis and the Malignant Phenotype. *Cancer Cell* **2005**, *8*, 241–254.
66. Chiquet, M.; Gelman, L.; Lutz, R.; Maier, S. From Mechanotransduction to Extracellular Matrix Gene Expression in Fibroblasts. *Biochim. Biophys. Acta, Mol. Cell Res.* **2009**, *1793*, 911–920.
67. Lämmermann, T.; Sixt, M. Mechanical Modes of 'Amoeboid' Cell Migration. *Curr. Opin. Cell Biol.* **2009**, *21*, 636–644.
68. Fackler, O. T.; Grosse, R. Cell Motility through Plasma Membrane Blebbing. *J. Cell Biol.* **2008**, *181*, 879–884.
69. Ingber, D. E. Can Cancer Be Reversed by Engineering the Tumor Microenvironment? *Semin. Cancer Biol.* **2008**, *18*, 356–364.

70. Yang, J. A.; Lohse, S. E.; Murphy, C. J. Tuning Cellular Response to Nanoparticles *via* Surface Chemistry and Aggregation. *Small* **2014**, *10*, 1642–1651.
71. Fan, D.; Takawale, A.; Lee, J.; Kassiri, Z. Cardiac Fibroblasts, Fibrosis and Extracellular Matrix Remodeling in Heart Disease. *Fibrog. Tissue Repair* **2012**, *5*, 15.
72. Lukes, A.; Mun-Bryce, S.; Lukes, M.; Rosenberg, G. A. Extracellular Matrix Degradation by Metalloproteinases and Central Nervous System Diseases. *Mol. Neurobiol.* **1999**, *19*, 267–284.
73. Bedossa, P.; Paradis, V. Liver Extracellular Matrix in Health and Disease. *J. Pathol.* **2003**, *200*, 504–515.
74. Lu, P.; Takai, K.; Weaver, V. M.; Werb, Z. Extracellular Matrix Degradation and Remodeling in Development and Disease. *Cold Spring Harbor Perspect. Biol.* **2011**, *3*, a005058.
75. Jana, N. R.; Gearheart, L.; Murphy, C. J. Seed-Mediated Growth Approach for Shape-Controlled Synthesis of Spheroidal and Rod-Like Gold Nanoparticles Using a Surfactant Template. *Adv. Mater.* **2001**, *13*, 1389–1393.
76. Jana, N. R.; Gearheart, L.; Murphy, C. J. Wet Chemical Synthesis of High Aspect Ratio Cylindrical Gold Nanorods. *J. Phys. Chem. B* **2001**, *105*, 4065–4067.
77. Gole, A.; Murphy, C. J. Polyelectrolyte-Coated Gold Nanorods: Synthesis, Characterization and Immobilization. *Chem. Mater.* **2005**, *17*, 1325–1330.
78. Grzincic, E. M.; Yang, J. A.; Drnevich, J.; Falagan-Lotsch, P.; Murphy, C. J. Global Transcriptomic Analysis of Model Human Cell Lines Exposed to Surface-Modified Gold Nanoparticles: The Effect of Surface Chemistry. *Nanoscale* **2015**, *7*, 1349–1362.